STRUCTURAL CHARACTERISATION AND LUMINESCENCE PROPERTIES OF PARAMAGNETIC Mn DOPED SnO$_2$ NANOPOWDERS OBTAINED VIA SIMPLE BUTHANOL ASSISTED SOL-GEL SYNTHESIS

A.-M. UNGUREANU[a], C. ANDRONESCU[a], G. VOICU[a], A. SCOBAN[a],
O. OPREA[a*], N. STANICA[b], I. JITARU[a]
[a]*University Politehnica of Bucharest, Faculty of Applied Chemistry and Materials Science, Bucharest, Romania*
[b]*Romanian Academy, "Ilie Murgulescu" Institute of Physical Chemistry, 202 Spl. Independentei, 060021, Bucharest, Romania*

We describe a simple approach to synthesize pure and manganese doped tin dioxide nanoparticles via a sol-gel method, starting from SnCl$_4$ and MnCl$_2$ in n-buthanol. The XRD analysis shows that well crystallized tetragonal SnO$_2$ was obtained, with a crystallite size of 4nm, when samples were calcined at 350°C. Optical investigation shows that the manganese doping in SnO$_2$ lattice leads to a decrease of the bang-gap energy due to the introduction of new unoccupied states by Mn *3d* electrons. The SnO$_2$ nanopowder exhibit strong blue-green luminescence, which indicate the presence of surface defects, such as oxygen vacancies. The emission intensity decreases as the dopant percent increases, indicating that manganese ions can block the blue-green emission by generating nonradiative decay channels or electron capture centres on the surface of nanocrystals. The magnetic susceptibility measurements show that the Mn ions are incorporated in the tin dioxide lattice, and that the samples are paramagnetic at room temperature.

1. Introduction

Tin dioxide is a wide gap semiconductor with many applications: sensor, catalyst, diluted magnetic semiconductor and therefore together with ZnO, TiO$_2$ and Fe$_3$O$_4$ it is one of the most studied oxides [1-16].

Recently, transition-metal doped tin dioxide has gained much attention due to the possibility of exhibiting room-temperature ferromagnetism. One of the favoured dopants is manganese, so there are many studies regarding the effect of Sn^{4+} substitution by manganese ions into the tin dioxide lattice.

There are various synthesis routes reported in literature [17-22] confirming that the structure and properties of manganese doped tin dioxide are highly influenced by the preparation method. Azam *et al.* investigated the electrical properties of Mn doped tin oxide nanoparticles obtained via sol-gel method, with manganese content varying from 0 to 15 mol % and reported a decrease in the crystallinity, crystallite size and lattice constant while increasing the manganese concentration [17]. Gopinadhan *et al.* reports room temperature ferromagnetism in manganese doped SnO$_2$ thin films prepared by spray pyrolysis method [18]. Also, manganese doped tin oxide thin films obtained through the same method were studied by Vadivel *et al.* [19]. Rajeeb Brahma et al. [20] demonstrated good transparency and conductivity in Mn-doped SnO2 films deposited by thermal evaporation on borosilicate glass substrates. Pulsed-laser deposition (PLD) is another method to fabricate Sn$_{1-x}$Mn$_x$O$_2$ films. This was used by H. Kimura *et al.* in their research in which

---

they obtained a rutile type oxide diluted magnetic semiconductor with high Mn concentrations ($x<0.34$). However, their studies report room temperature paramagnetic behaviour of the material [21]. *Z.M. Tian et al.* synthesized Mn doped tin dioxide nanoparticles with the dopant concentration range between 0-7% at by chemical co-precipitation method. They report that manganese ions incorporate in the tin dioxide lattice as a mixture of Mn^{3+} and Mn^{4+}. Room temperature ferromagnetism is observed for samples with Mn concentration under 5% at and calcined at 450^oC with strong correlation to the surface structural defects [22].

Although many researchers have investigated the properties of Mn doped tin dioxide, there are inconsistent results concerning the magnetic behaviour of this material and the mechanism of its occurrence. Most studies investigate the properties of doped tin dioxide thin films, but there are not many reports concerning the properties of nanopowders. In the present work, we report the synthesis of manganese doped tin dioxide nanopowders using an improved buthanol assisted sol-gel method. This route has the advantage of being simple and economical as no alkoxides are used. The dopant concentration in the synthesized samples varies in the range 0-5% at. The samples were investigated by spectroscopic methods: XRD, XPS, UV-VIS, FTIR and PL. The samples show paramagnetic behaviour at room temperature, as determined by susceptibility measurements carried out with Faraday Balance.

2. Experimental details

2.1 Experimental procedure

Manganese doped tin dioxide nanoparticles were obtained by a simple buthanol assisted sol-gel method, presented in Fig. 1. The 0%, 2% and 5% at. Mn doped samples were obtained using $SnCl_4$ (99.99%) and $MnCl_2 \cdot 4H_2O$ salts. The salts were mixed in buthanol under magnetic stirring. A 1:1 ammonia solution was added under stirring drop wise until a neutral pH was reached. The samples were kept under stirring for another 30 minutes, to make sure that the sol is properly formed. All three samples were left to age in laboratory conditions for 6 days. The gels were centrifuged in distilled water in order to remove residual ions such as Cl^-. The solid was collected and dried at 105^oC. The dried gels were subjected to a thermal treatment carried out at 350^oC for 2 hours, with a heating rate of 10^oC/minute.
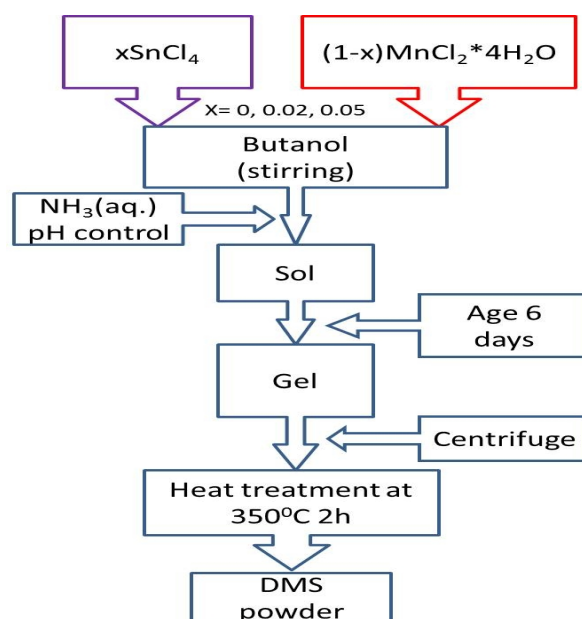
Fig. 1. - *Synthesis scheme of Mn doped SnO₂*

The heat treatment temperature was choosen based on the information from the thermal analysis, figure 2.
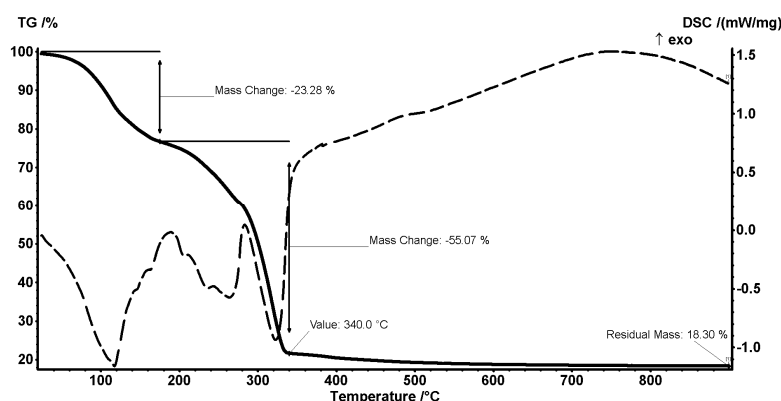
Fig. 2. The thermal analysis of tin dioxide precursor

2.2. Experimental techniques

a) X-ray Diffraction. X-ray powder diffraction patterns were obtained with a Shimadzu XRD6000 diffractometer, using Cu Kα (1.5406 Å) radiation operating with 30 mA and 40 kV in the 2θ range 10–70°. A scan rate of 1° min^{-1} was employed.

b) X-ray Photoelectron Spectroscopy. XPS spectra were obtained with a Sigma Probe ThermoVG spectrometer with an excitation source of Al Kα = 1486.6 eV.

c) Infrared Spectroscopy. The Fourier transform infrared (FTIR) spectra were recorded using the KBr pellet technique on a Bruker Tensor 27 spectrometer in the 4000–400 cm^{-1} frequency range. A total of 30 scans and a resolution of 1 cm^{-1} were employed in getting the spectra.

d) Diffuse reflectance spectra measurements were made with a JASCO V560 spectrophotometer with solid sample accessory, in the domain 200-800nm, with a speed of 200nm·min^{-1}.

e) Photoluminescence spectra. Photoluminescence spectra (PL) were measured with a Perkin Elmer P55 spectrometer using a Xe lamp as a UV light source at ambient temperature. An excitation wavelength of 320 nm was used.

f) Magnetic susceptibility measurements were carried at room temperature with a Faraday balance.

g) Thermal analysis. Thermal behaviour of the tin dioxide precursor was followed by TG-DSC with a Netzsch TG 449C STA Jupiter. Sample was placed in alumina crucible and heated with 10K·min^{-1} from room temperature to 900° C, under the flow of 10 mL min^{-1} dried air.

3. Results and discussions
XRD Analysis

XRD patterns of the 0-5% at. Mn doped tin dioxide samples are presented in figure 3. All peaks can be clearly indexed to tetragonal SnO_2 as per JCPDS file 77-0447. The lack of secondary phases, as well as the slight shift of the maximums suggests a good incorporation of dopant ions into the tin dioxide lattice. The broadness of the peaks suggests nanometric crystallites characterised by the presence of structural defects.
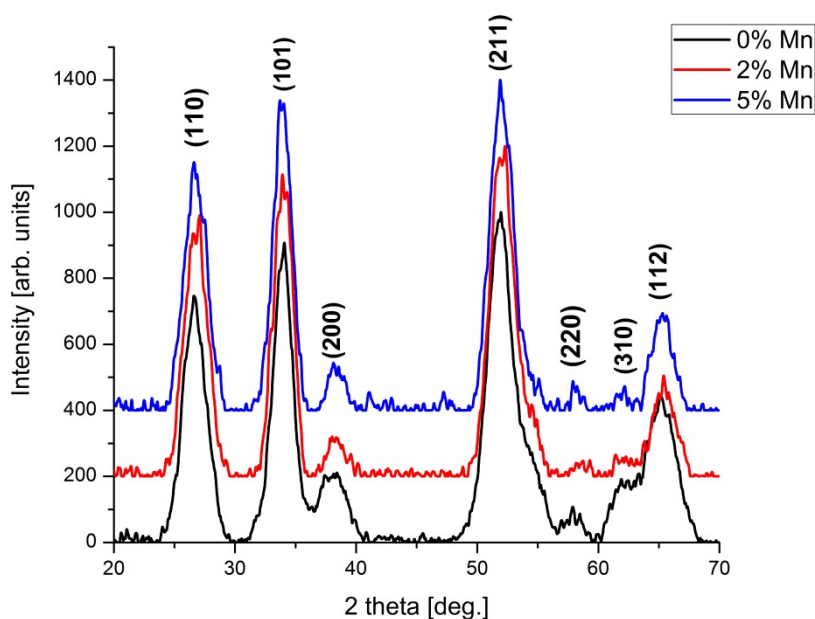
Fig. 3. XRD patterns for SnO$_2$ doped with cu 0%, 2% and 5% Mn

The mean crystallite sizes were calculated with Sherrers formula using the most intense three peaks. Their values are presented in Table I along with the calculated values of lattice parameters *a* and *c* and the cell volumes. The crystallite size is not influenced by the incorporation of manganese ions. However, the variation of lattice parameters confirms the presence of the manganese ions in the host lattice in different oxidation states, as further demonstrated by XPS.

Table I. Crystallite size and lattice parameters for 0%,2% and 5% Mn doped SnO$_2$

Sample	Crystallite size [nm]	Lattice parameters [Å]		Cell Volume [Å^3]
		a	c	
0% Mn	4.3	4.726	3.178	70.98
2% Mn	4.1	4.702	3.176	70.22
5% Mn	4.1	4.707	3.188	70.63

XPS Spectroscopy

XPS analysis was performed in order to investigate the chemical state of the surface of 0%, 2% and 5% Mn doped tin dioxide nanopowders. All spectra were calibrated with respect to C 1s adventitious peak at 284.8 eV. Table II summarizes the data obtained through XPS. The survey spectra are shown in figure 4. All three samples show similar spectra that are typical for tin dioxide. Mn 2p peak is not visible on survey scan due to the low dopant concentration.

High resolution spectra (figure 5a) for Sn 3d reveal binding energy peaks at 487.3 eV, 486.7 eV and 486.6 eV for Sn 3d$_{5/2}$ and doublet energy separation values of 8.4- 8.5 eV (Table II). These values clearly show that Sn^{4+} state is present in all samples [22, 23].

O 1s binding energy peaks are located at 531.2 eV, 531.1 eV and 530.6 eV for 0%, 2% and 5% Mn doped samples. These peak values are attributed to lattice O^{2-} in tin dioxide. The broadness of the peaks suggests the presence of –OH groups on the surface in accordance with FT-IR analysis.

Table II. XPS binding energy peaks and doublet separation values

Sample / Binding energy peaks [eV]	Sn $3d_{3/2}$	Sn $3d_{5/2}$	Energy separation in doublet [eV]	O 1s	Mn $2p_{1/2}$	Mn $2p_{3/2}$	Energy separation in doublet [eV]	Surface Chemical Composition
0% Mn	495.7	487.3	8.4	531.2	-	-	-	$SnO_{1.58}$
2 % Mn	495.3	486.7	8.4	531.1	653.1	641.9	11.2	$Sn_{0.984}Mn_{0.016}O_{1.48}$
5 % Mn	495.1	486.6	8.5	530.6	652.7	641.0	11.7	$Sn_{0.981}Mn_{0.019}O_{1.43}$
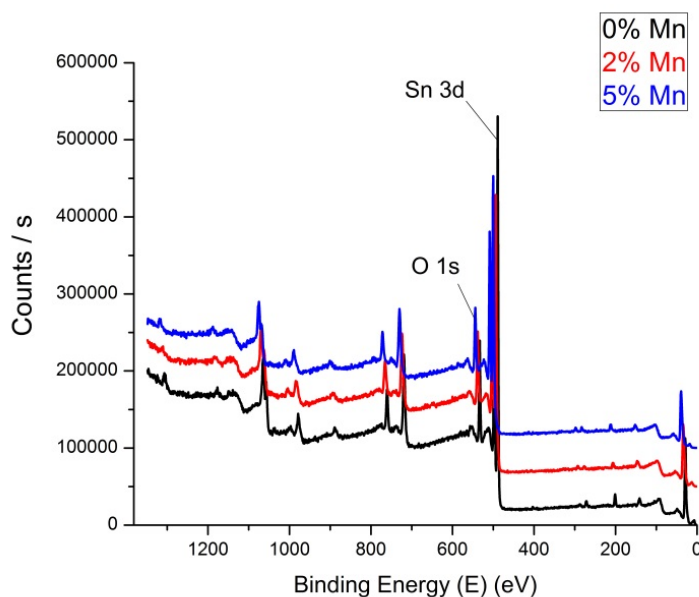
Fig. 4. XPS survey spectra for pure and Mn doped tin dioxide
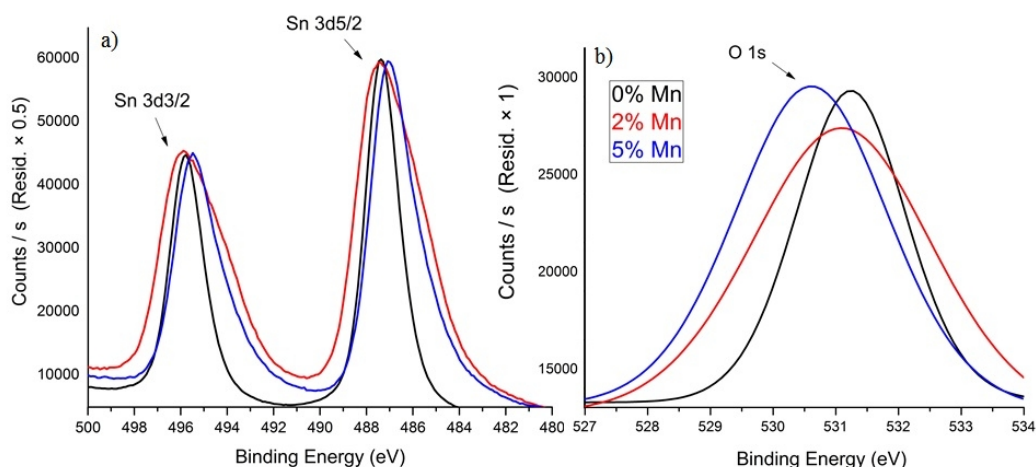
Fig. 5. High resolution spectra for a) Sn3d dublet, b) O 1s

Figure 6 shows the Mn 2p high resolution spectra for 2% and 5% Mn doped samples. For the 2% sample the Mn 2p3/2 binding energy peak is located at 641.9 eV with a doublet separation of 11.2 eV, showing that in this sample manganese is found on the surface mostly in a Mn^{3+} state. For the 5% sample the Mn 2p3/2 binding energy peak is located at 641.0 eV with a doublet separation of 11.7 eV. This clearly shows that the oxidation state of the doping ion is different,

being mostly Mn^{2+} [23-26]. These results are consistent with cell volume evolution determined through XRD.
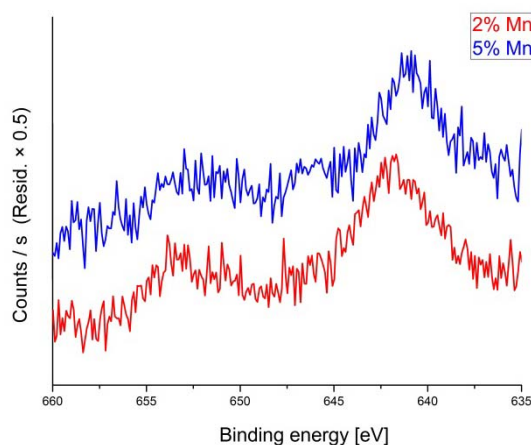
Fig. 6. Mn 2p high resolution spectra

Chemical surface composition determined through XPS is presented in Table 2. All samples are characterized by a nonstoichiometric composition and the presence of oxygen vacancies. However, manganese ions are present on the surface only in 1.6 at % and 1.9 at %. The amount of oxygen vacancies increases with dopant concentration, as per charge compensation.

FT-IR Spectroscopy

FT-IR spectra confirm good decomposition of organic phase at 350°C for all samples. The absorption bands around 3426 cm^{-1} are assigned to –OH groups and the bands around 1624 cm^{-1} are assigned to fundamental water vibration, as the samples were not recorded in-situ. The peaks found around 1410 cm^{-1} for all samples are assigned to Sn-O-Sn bridges formed through condensation of Sn-OH bonds on the surface [27].

FT-IR spectra for the manganese-doped samples were recorded between 4000-400 cm^{-1} and are presented in figure 7. They were compared to an undoped sample obtained through the same method.
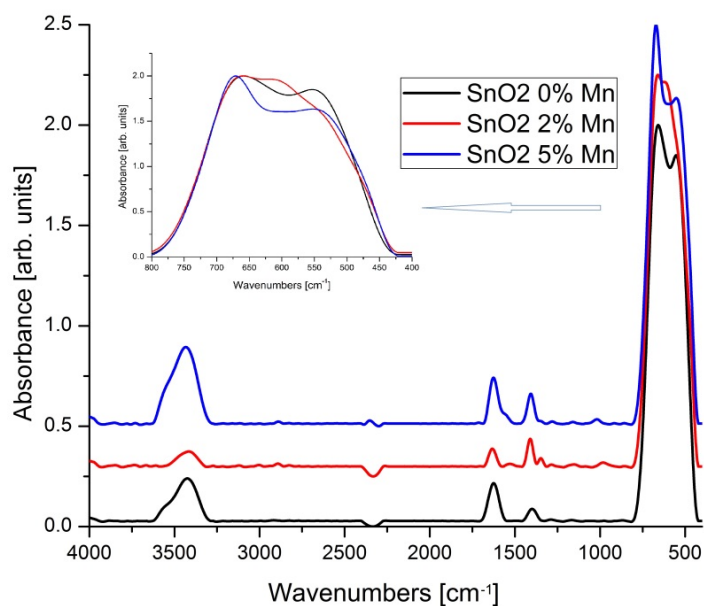
Fig. 7. FT-IR absorbance spectra recorded for 0%, 2% and 5% Mn doped SnO$_2$.
Inset: 800-400 cm^{-1} region of the spectra

The intense asymmetric bands in the region 700-400 cm^{-1} (inset) are characteristic for polycrystalline tin dioxide [27-30]. It can be clearly observed that the intensity of these bands increases with increasing the dopant concentration. Moreover, -OH groups on the sample surface influence the shape and the maximum positions of the absorption bands.

UV-VIS Spectroscopy
UV-VIS spectra for all three doped samples are presented in Figure 8a. It can be clearly observed that 2% and 5% Mn samples exhibit a red shift compared to the undoped sample. This behaviour can be associated with an increased density of states in the semiconductor gap. The higher absorbance in the visible region is due to the incorporation of Mn ions in the tin dioxide lattice.

a   b
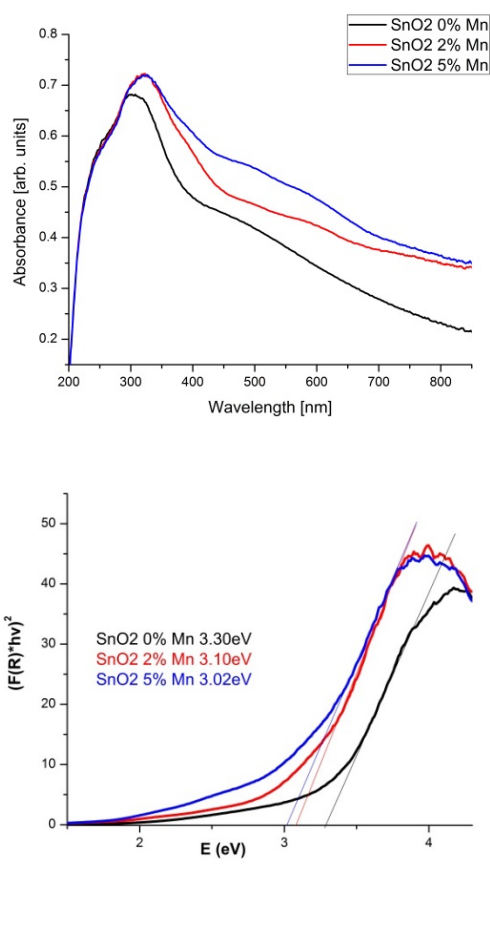
Fig. 8. a) UV-VIS spectra obtained for 0%, 2% and 5% Mn doped SnO$_2$ nanoparticles
b) Tauc plot of (F(R)*hv)^2 vs photon energy with calculated band gaps

For analysis purposes the diffuse reflectance, *R*, of the sample can be related to the Kubelka-Munk function *F(R)* by the relation F(R)=(1-R)^2/2R, [31]. To determine the band-gap energies (Eg) for the tin dioxide nanoparticles, a plot of the square of the modified Kubelka-Munk function vs. the energy is presented in the figure 8b. This yields the direct band gap energy. Adopting the method proposed by Cao et al., [32] the band-gap energies (Eg) for the tin dioxide nanoparticles were determined. The values were compared with the band gap value for undoped tin dioxide, calculated through the same method [33]. All calculated values are smaller than the bulk value (3.6 eV). While comparing the Eg values of undoped and doped samples, a decrease is observed. This decrease sharpens with the increase of Mn concentration for 2% and 5% Mn samples. Most probably, this behaviour is caused by the occurrence of additional electronic levels inside the band gap, because of Mn incorporation in the SnO$_2$ lattice.

Luminescence spectra

The luminescence spectra, figure 9, show that the 0%, 2% and 5% Mn doped SnO_2 samples have a similar structure, with an emission in UV region, around 386nm, and two blue-green emissions, one centred at 457 nm (with shoulders at 446 and 434 nm) and second at 482 nm. The weak green emission is present around 513-526 nm.

The UV emission corresponds to the near band edge emission (due to the radiative annihilation of excitons) and the visible emission is commonly referred to as a deep-level or trap-state emission. The relative strength of UV to Vis emissions exhibits a dramatic threshold dependence on surface morphology and near-surface defects.

The emission in the blue-green range (bands at 434, 446, 457, 482, and 513 nm) are defect-related emissions, generated by the oxygen vacancies.

The increase in the Mn(II) ions percentage has a direct effect on the intensity of the blue and violet emission. The decrease in intensity takes place systematically, which confirms the correlation between doping percentage and emission intensity. According to literatures, the quenching of the blue emission is caused by the apparition of electron capture centres on the surface of nanocrystals or the existence of nonradiative decay channels [34]. This behaviour can be correlated with the presence of manganese ions on the surface of the nanoparticles.
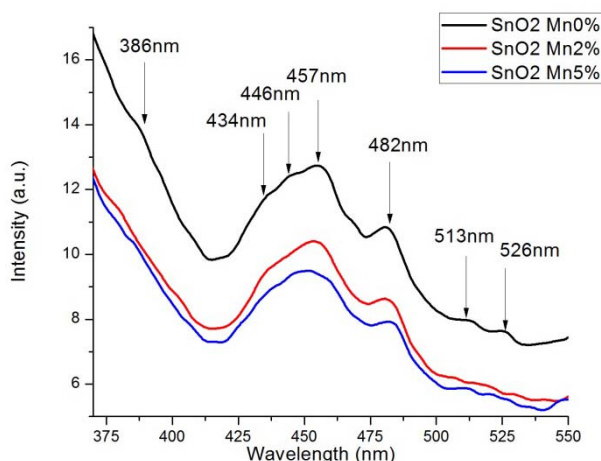
Fig. 9. Photoluminescence spectra of 0%, 2% and 5% Mn doped SnO₂ nanoparticles

Magnetic susceptibility

The magnetic susceptibility measurements show that the Mn ions are incorporated in the tin dioxide lattice, and that the samples are paramagnetic at room temperature.

Table III. Effective magnetic moments - experimental values

Sample	T [K]	μ_{eff} [M.B]
$SnO_{1.58}$	293	diamagnetic
$Sn_{0.984}Mn_{0.016}O_{1.48}$	293	0.75
$Sn_{0.981}Mn_{0.019}O_{1.43}$	293	0.77

The influence of the dopant concentration, as well as the dopant oxidation state is reflected by the variation of the magnetic moments, which are increasing with the increase of manganese concentration as presented in Table III. The values of magnetic susceptibilities are in agreement with XPS analysis.

4. Conclusions

A synthetic method for the undoped tin dioxide and manganese-doped tin dioxide nanopowders using n-buthanol has been presented. The thermal analysis of the precursor gel

indicated a thermal treatment temperature of 350°C for 2 hours. The manganese ions were incorporated in the tin dioxide lattice with no influence over the crystallite size (4 nm), XRD analysis indicating existence of a single phase compound, tetragonal tin dioxide. XPS analysis indicates high oxygen vacancy surfaces for all samples. The manganese ions incorporate in 3$^+$ and 2$^+$ states with low surface concentration and paramagnetic behaviour at room temperature, the value of μ_{eff} increasing with the manganese content.

The samples exhibited blue-green photoluminescence by the UV excitation, the presence of manganese ions quenching the emission. The band gap value of doped samples is smaller than the band gap value of the bulk tin dioxide.

Acknowledgments

References

[1] C.I. Covaliu, T. Mălăeru, G. Georgescu, O. Oprea, L. Alexandrescu, I. Jitaru –
Dig J Nanomater Bios., **6**(4), 1491 (2011)

[2] D. Ficai, A. Ficai, B. S. Vasile, M. Ficai, O. Oprea, C. Guran, E. Andronescu –
Dig J Nanomater Bios., **6**(3), 943 (2011)

[3] C.I. Covaliu, L. C. Chioaru, L. Crăciun, O. Oprea, I. Jitaru – Optoelectron. Adv. Mater.
– Rapid Comm., **5** (10), 1097 (2011)

[4] A. Ianculescu, F. Prihor Gheorghiu, P. Postolache, O. Oprea, L.Mitoseriu –
Journal of Alloys and Compounds **504**(2), 420 (2010)

[5] F. Vaja (Dumitru), D. Ficai, A. Ficai, O. Oprea, C. Guran – J. Optoelectron. Adv. Mater.
15(1- 2), 107 (2013)

[6] Johannes B, Torsten N, Nina JB, Lars PHJ, Udo W, Tuan AD, et al., Biointerface research in
applied chemistry, **2**(4), 380 (2012)

[7] Grumezescu AM, Andronescu E, Ficai A, Mihaiescu DE, Vasile BS, Bleotu C., Letters in
Applied NanoBioScience **1**(2), 31 (2012)

[8] F. Vaja (Dumitru), C. Comanescu, O. Oprea, D. Ficai, C. Guran - Revista de Chimie
63(7), 722 (2012)

[9] O. Oprea, O. R. Vasile, G. Voicu, L. Craciun, E. Andronescu - Dig J Nanomater Bios.
7(4), 1757 (2012)

[10] Mihaiescu DE, Horja M, Gheorghe I, Ficai A, Grumezescu AM, Bleotu C, et al., Letters in
Applied NanoBioScience, **1**(2), 45 (2012)

[11] Grumezescu AM, Andronescu E, Ficai A, Yang C-H, Huang K, Vasile BS, et al. Letters in
Applied NanoBioScience **1**(3), 56 (2012)

[12] O. Oprea, E. Andronescu, B.S. Vasile, G. Voicu, C. Covaliu, Dig J Nanomater Bios.
6(3)**,** 1393 2011)

[13] Grumezescu AM, Andronescu E, Ficai A, Bleotu C, Mihaiescu DE, Chifiriuc MC.,
International Journal of Pharmaceutics, **436**(1-2), 771 (2012)

[14] O Oprea, O. R. Vasile, G. Voicu, L. Craciun, E. Andronescu - Dig J Nanomater Bios.
7(4), 1757 (2012)

[15] O.R. Vasile, E. Andronescu, C. Ghitulica, B.S. Vasile, O. Oprea, E. Vasile, R. Trusca –
Journal of Nanoparticle Research, **14** (12), art. no. 1269, (2012)

[16] O Oprea, O. R. Vasile, G. Voicu, E. Andronescu - Dig J Nanomater Bios. – **8**(2), 747 (2013)

[17] Ameer Azam, Arham S. Ahmed, M. Chaman, A. H. Naqvi, Journal of Applied Physics,
108, 094329 (2010)

[18] K. Gopinadhan, Subhash C. Kashyap, Dinesh K. Pandya, and Sujeet Chaudharya, Journal of
Applied Physics, **102**, 113513 (2007)

1178

[19] K.Vadivel, V.Arivazhagan, S.Rajesh, International Journal of Scientific & Engineering Research, **2**(4), 43 (2011)

[20] Rajeeb Brahma, M Ghanashyam Krishna, A K Bhatnagar, Bull. Mater. Sci., **29**(3), 317 (2006)

[21] H. Kimura, T. Fukumura, M. Kawasaki, K. Inaba, T. Hasegawa, Applied Physics Letters, **80**(1), 94 (2002)

[22] Z.M. Tian, S.L. Yuan, J.H. He, P. Li, S.Q. Zhang, C.H. Wang, Y.Q. Wang, S.Y. Yin, L. Liu, Journal of Alloys and Compounds **466**(1-2), 26 (2008)

[23] Yuhua Xiao, Shihui Ge, Li Xi, Yalu Zuo, Xueyun Zhou, Bangmin Zhang, Li Zhang, Chengxian Li, Xiufeng Han, Zhenchao Wen, Applied Surface Science **254**(22), 7459 (2008)

[24] M. Kantcheva, M.U. Kucukkal, S. Suzer, Journal of Molecular Structure **482–483,** 19 (1999)

[25] K. M. Reddy, J. Hays, S. Kundu , L. K. Dua, P. K. Biswas, C. Wang, V. Shutthanandan, M. H. Engelhard, X. Mathew, A. Punnoose, J Mater Sci: Mater Electron, 18:1197 (2007)

[26] H.W. Nesbitt, D. Banerjee, American Mineralogist, **83**, 305 (1998)

[27] D. Amalric-Popescu, F. Bozon-Verduraz, Catalysis Today **70**, 139 (2001)

[28] Mauro Epifani, Maro Alvisi, Gabriella Leo, J. Am. Ceram. Soc., **84**(1), 48 (2001)

[29] S. Gnanam, V. Rajendran, J Sol-Gel Sci Technol 53:555 (2010)

[30] Feng Gu, Shu Fen Wang, Meng Kai Lu, Yong Xin Qi, Guang Jun Zhou, Dong Xu, Duo Rong Yuan, Inorganic Chemistry Communications **6,** 882 (2003)

[31] G. Kortum, Reflectance Spectroscopy, Springer-Verlag, New York, 1969

[32] G. Cao, L.K. Rabenberg, C.M. Nunn, T.E. Mallouk, Chem. Mater., **3**, 149 (1991)

[33] J. Tauc, R. Grigorovici and A. Vancu, Phys. Status Solidi, **15**, 627 (1966)

[34] G. Voicu, O. Oprea, B.S. Vasile, E. Andronescu, Dig J Nanomater Bios., **8**(2), 667 (2013)